Conclusions

In the present work, a methodology for three-dimensional structured multiblock grid generation in axial turbomachinery was presented. There is a main O grid around each blade, constructed by stacking two-dimensional blade-to-blade surface O grids generated biharmonically. Only a few user-defined parameters are needed for generating the blade-to-blade surface O grids, and experience has shown that the choice of these parameters is a quite straightforward task. Biharmonic grid generation ($\nabla^4\xi=0$, $\nabla^4\eta=0$) has the decisive advantage over elliptic grid generation ($\nabla^2\xi=Q_\xi$, $\nabla^2\eta=Q_\eta$) in that it allows automatic control of both position and orthogonality at the boundaries. The numerical implementation used ($\nabla^2\xi=Q_\xi$, $\nabla^2 Q_\xi=0$; $\nabla^2\eta=Q_\eta$, $\nabla^2 Q_\eta=0$) clearly shows that biharmonic grid generation computes the source terms Q_ξ and Q_η, which are user-defined in Poisson grid generation. The biharmonic solver gives a quasiorthogonal initial grid that is not yet refined near the solid walls. Stretching to accurately resolve boundary layers is obtained by interpolating points on computed grid lines.

Tip-clearance gaps are meshed using O-type grids, generated biharmonically. The radial surfaces of the main blade-to-blade surface O grid are stretched near the casing and the hub. The clearance-gap TC grid is stretched both at the casing and at the blade tip. The radial distribution of the TC grid is independent of the radial distribution of the O grid. A buffer OZ grid that overlaps with the O grid, and that is stretched both at the casing and at the blade tip, is used to accurately resolve the flow coming over the tip.

The method is quite robust and provides good-quality structured grids. It has been applied to the computation of various compressor and turbine configurations using a three-dimensional Navier–Stokes solver with multiequation turbulence closures.[3,9] In the case of stators with clearance gap at the hub, grid generation is done in an exactly analogous way.

Appendix: Geometric Stretching

The geometric stretching used stretches N_1 of the N points near the starting location [$s_1=s(1)=0$] with ratio r_1, stretches N_2 points near the final location [$s_2=s(N)=L$] with ratio r_2, and places $N-N_1-N_2$ equidistant points in between:

$$l_{gs}(n, L, N, N_1, r_1, N_2, r_2)=\begin{cases} s(1)+\dfrac{r_1^{n-1}-1}{r_1-1}hr_1^{-(N_1-2)}, & n=2,\ldots,N_1 \\ s(N_1)+(n-N_1)h, & n=N_1+1,\ldots,N-N_2+1 \\ s(N-N_2+1)+\dfrac{r_2^{-(n-N+N_2-1)}-1}{r_2^{-1}-1}h, & n=N-N_2+2,\ldots,N \end{cases} \tag{A1}$$

$$h=L\left[N-N_1-N_2+1+\frac{r_1^{-(N_1-1)}-1}{r_1^{-1}-1}+\frac{r_2^{-(N_2-1)}-1}{r_2^{-1}-1}\right]^{-1} \tag{A2}$$

References

[1]Dawes, W. N., "The Simulation of 3-D Viscous Flow in Turbomachinery Geometries Using a Solution-Adaptive Unstructured Mesh Methodology," *Journal of Turbomachinery*, Vol. 114, July 1992, pp. 528–537.

[2]Basson, A. H., Kunz, R. F., and Lakshminarayana, B., "Grid Generation for 3-D Turbomachinery Geometries Including Tip Clearance," *Journal of Propulsion and Power*, Vol. 9, No. 1, 1993, pp. 59–66.

[3]Gerolymos, G. A., Tsanga, G., and Vallet, I., "Near-Wall k-ϵ Computation of Transonic Turbomachinery Flows with Tip-Clearance," *AIAA Journal*, Vol. 36, No. 10, 1998, pp. 1769–1777.

[4]Thompson, J. F., Thames, F. C., and Mastin, C. W., "Automatic Numerical Generation of Body-Fitted Curvilinear Coordinate System for Field Containing any Number of Arbitrary 2-D Bodies," *Journal of Computational Physics*, Vol. 15, 1974, pp. 299–319.

[5]Steger, J. L., and Sorenson, R. L., "Automatic Mesh-Point Clustering near a Boundary in Grid Generation with Elliptic Partial Differential Equations," *Journal of Computational Physics*, Vol. 33, 1979, pp. 405–410.

[6]Sparis, P. D., "A Method for Generating Boundary-Orthogonal Curvilinear Coordinate Systems Using the Biharmonic Equation," *Journal of Computational Physics*, Vol. 61, 1985, pp. 445–462.

[7]Sparis, P. D., and Karkanis, A., "Boundary-Orthogonal Biharmonic Grids via Preconditioned Gradient Methods," *AIAA Journal*, Vol. 30, No. 3, 1992, pp. 671–678.

[8]Fottner, L. (ed.), "Test Cases for Computation of Internal Flows in Aero Engine Components," AGARD Advisory Rept. 275, 1990, pp. 124–138.

[9]Gerolymos, G. A., and Vallet, I., "Tip-Clearance and Secondary Flows in a Transonic Compressor Rotor," *Journal of Turbomachinery* (to be published).

Adaptive Analysis of Oscillating Cascade Flows on a Quadrilateral–Triangular Mesh

S. Y. Yang*

National Huwei Institute of Technology, Yunlin 632, Taiwan, Republic of China

Introduction

In recent years, a number of Euler[1,2] and Navier–Stokes[3,4] solvers have been presented to simulate the blade vibration problems. Wolff and Fleeter[1] applied the Fourier series lagged boundary condition treatment on an expanded grid along the periodic boundary. Hwang and Yang[2] presented a rigid-deformable dynamic mesh algorithm to investigate transonic flows around an oscillating cascade of four blades. On a multipassage computational mesh,[3] the explicit four-stage Runge–Kutta scheme and the Baldwin–Lomax mixing-length turbulence model were adopted. The calculation showed that there was a more apparent mesh dependence of the results in the regions of flow separation. Within a composite grid where a deforming C-grid was embedded in an H-grid, a coupled inviscid/viscous model[4] was implemented to incorporate the inverse integral boundary-layer solution and the time-marching NPHASE analysis. The purpose of this work is to present a solution-adaptive solver to investigate the transonic oscillating cascade flows on a quadrilateral–triangular mesh. The Euler equations with moving domain effects are solved in the Cartesian coordinate. This solver

Received June 1, 1998; presented as Paper 98-3436 at the AIAA/ASME/SAE/ASEE 34th Joint Propulsion Conference, Cleveland, OH, July 13–15, 1998; revision received Dec. 3, 1998; accepted for publication Dec. 4, 1998.

*Associate Professor, Department of Aeronautical Engineering. Member AIAA.

includes the locally implicit total variation diminishing scheme, dynamic mesh algorithm,[2] interpolation method, two-level refinement procedure,[5] and enrichment indicator.

Adaptive-Mesh Technique

The present adaptive-mesh technique includes the mesh enrichment indicator, two-level refinement procedure, and interpolation method. In the present calculations, the absolute value of the substantial derivative of Mach number $|DM/Dt|$ is chosen as the mesh enrichment indicator. As for the two-level refinement procedure, the mesh enrichment is operated on the background grid (initial grid) instead of the last adapted mesh. Initially, the value of $|DM/Dt|$ of each unrefined cell is calculated. The product of a specified constant C_1 and the average value of $|DM/Dt|$ over the entire background grid is selected as the first threshold value. If the value of $|DM/Dt|$ of each unrefined cell is larger than the first threshold value $C_1 * |DM/Dt|_{av}$, the new node will be placed at the midpoint of each edge of the quadrilateral–triangular cell or the center of the quadrilateral cell.[5] After finishing the first-level refinement, the properties at all added new nodes are interpolated from those at the background nodes. Continuing the second-level mesh refinement, the value of $|DM/Dt|$ for each cell on the intermediate mesh and the corresponding second threshold value $C_2 * |DM/Dt|_{av}$ are computed. Then the intermediate mesh is refined by processing the first-level refinement technique.

Results and Discussion

In the present calculations, the inlet Mach number and exit pressure ratio are set to be 0.8 and 0.7322, respectively. The computational domain contains four uncambered biconvex blades, where the values of thickness-to-chordratio, solidity, and stagger angle are 0.076, 1.3, and 53 deg, respectively. The motion of these four blades, which is executing torsional mode oscillations about midchord, is governed by the following:

$$\alpha = \alpha_0 + \alpha_I \sin(2Mk\upsilon + m\sigma) \tag{1}$$

where α, α_0, α_I, M, k, υ, and σ represent the instantaneous angle of attack, mean flow angle of attack, oscillation amplitude, inlet Mach number, reduced frequency, and nondimensionalized time scale and interblade phase angle, respectively. The blade numbers $m = 0$, 1, 2, and 3 represent each blade from the lowest to the highest one, respectively. As shown in Fig. 1, the quadrilateral–triangular mesh contains 13,830 elements and 9619 nodes. The periodic solution is achieved by processing six cycles of motion, and it takes 3600 time steps to accomplish one cycle of motion. C_1 and C_2 are set to be 0.5 and 2.5, respectively, and adaptation is performed every 36 time steps. If adaptation is performed every 15 time steps, an identical result will be obtained. The present solution is calculated on a Dec-3000 workstation, and it takes 13.7 computational seconds per iteration.

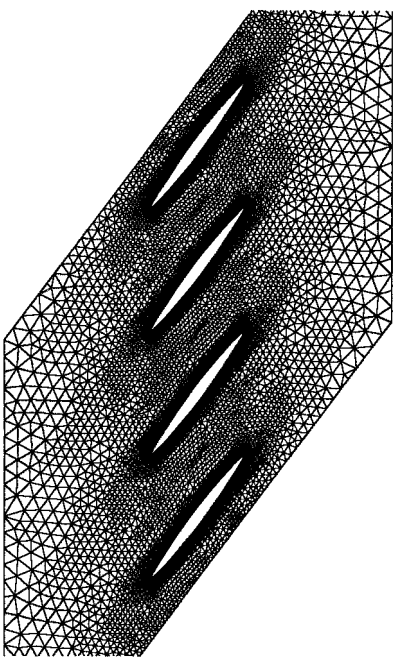

Fig. 1 Partial view of the quadrilateral–triangular mesh (13,830 elements and 9619 nodes).

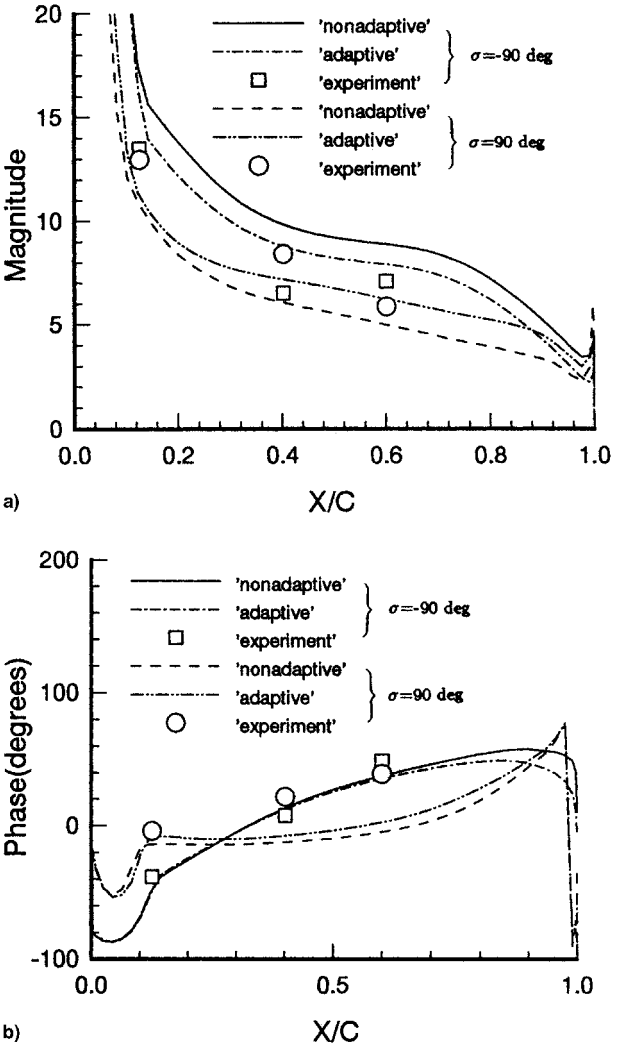

Fig. 2 a) Magnitude and b) phase angle of the first harmonic dynamic pressure difference coefficient ΔC_p for an oscillating cascade of four blades (k = 0.462, α_0 = 7 deg, and α_I = 1.2 deg).

When one value of α_I (1.2 deg) and two values of σ (-90 and 90 deg) are chosen, magnitudes and phase angles of the first harmonic dynamic surface pressure difference coefficient ΔC_p are calculated and plotted in Fig. 2. To evaluate the present adaptive solver, the experimental data[6] and Euler solutions obtained on the nonadaptive quadrilateral–triangular mesh[2] are adopted for comparison. By choosing the experimental data as the reference values, the distributions of magnitude in Fig. 2a indicate that the present adaptive solver provides better results than does the nonadaptive approach. For the phase-angle distributions with σ equal to 90 deg in Fig. 2b, the same conclusion is drawn. When the value of σ is replaced by -90 deg, the difference between adaptive and nonadaptive results is slight, and both solutions compare well with the experimental data.

As for the case with σ and α_I equal to 90 and 4.8 deg, respectively, the instantaneous mesh and Mach number contour ($2Mk\upsilon = 12\pi$)

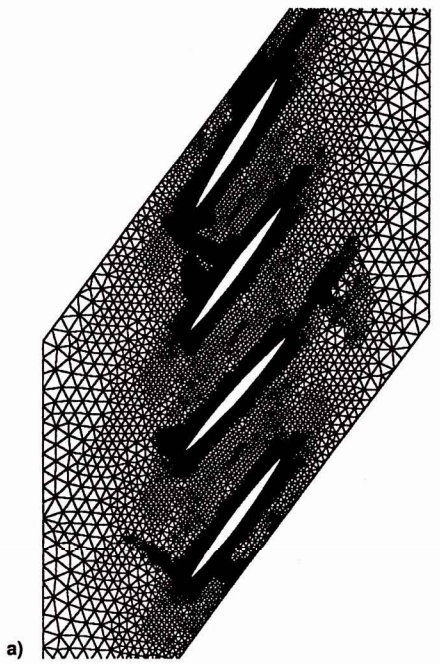

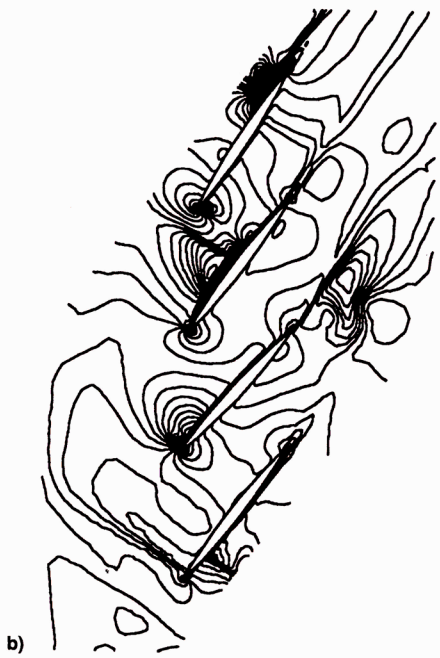

Fig. 3 a) Instantaneous mesh and b) Mach number contour for an oscillating cascade of four blades (k = 0.462, α_0 = 7 deg, α_I = 4.8 deg, σ = 90 deg, and $2Mk\tau = 12\pi$).

are plotted in Fig. 3. From the results given in Fig. 3, shocks appear on the front part of the upper surface of the second blade, and on the midchord of the upper surface of the third blade. Meanwhile, a compression wave on the upper leading edge of the lowest blade is observed. Within the passage between the lowest and highest blades, a shock is depicted that is strong enough to choke the flowfield.

Conclusions

In the present work, a solution-adaptive approach has been presented to investigate the transonic oscillating cascade flows. In a Cartesian coordinate system, the unsteady Euler equations are solved. Comparing the distributions of magnitude and phase angle of the first harmonic dynamic pressure difference coefficient, the present adaptive solutions show better agreement with the experimental data than those from the nonadaptive approach. From the comparison and discussion of instantaneous mesh and Mach number, it is evident that the present adaptive mesh clearly captures the unsteady wave behavior.

References

[1]Wolff, J. M., and Fleeter, S., "Single-Passage Euler Analysis of Oscillating Cascade Aerodynamics for Arbitrary Interblade Phase," *Journal of Propulsion and Power*, Vol. 10, No. 5, 1994, pp. 690–697.

[2]Hwang, C. J., and Yang, S. Y., "Inviscid Analysis of Transonic Oscillating Cascade Flows Using a Dynamic Mesh Algorithm," *Journal of Propulsion and Power*, Vol. 11, No. 3, 1995, pp. 433–440.

[3]He, L., "Unsteady Flow in Oscillating Turbine Cascade Part 2. Computational Study," American Society of Mechanical Engineers, Paper 96-GT-375, June 1996.

[4]Wolff, J. M., and Fleeter, S., "Nonlinear Separated Inviscid-Viscous Analysis of Oscillating Cascade Aerodynamics Using an Inverse Integral Method," American Society of Mechanical Engineers, Paper 97-GT-85, June 1997.

[5]Hwang, C. J., and Fang, J. M., "Solution-Adaptive Approach for Unsteady Flow Calculations on Quadrilateral-Triangular Meshes," *AIAA Journal*, Vol. 34, No. 4, 1996, pp. 851–853.

[6]Buffum, D. H., and Fleeter, S., "The Aerodynamics of an Oscillating Cascade in a Compressible Flowfield," *Journal of Turbomachinery*, Vol. 112, No. 4, 1990, pp. 759–767.

Theoretical Prediction of Mean Droplet Size of Y-Jet Atomizers

H. S. Couto,* J. A. Carvalho Jr.,† and D. Bastos-Netto‡
National Space Research Institute
12630-000 Cachoeira Paulista, Brazil
M. Q. McQuay§
Brigham Young University, Provo, Utah 84602
and
P. T. Lacava¶
National Space Research Institute
12630-000 Cachoeira Paulista, Brazil

Nomenclature

C_d	= discharge coefficient, nondimensional
D_0	= mixing chamber diameter, m
d_l	= ligament diameter, m
f	= constant, nondimensional
h_0	= liquid sheet thickness at the nozzle tip, m
K	= nozzle parameter, defined in Eq. (5), ms
l_0	= mixing chamber length, m
m_{air}	= atomizing airflow rate, kg s^{-1}
m_f	= mass flow rate of liquid, kg s^{-1}
P_c	= chamber pressure, Pa
P_s	= ambient pressure, Pa
P_0	= stagnation pressure, Pa

Received Feb. 21, 1998; revision received Dec. 30, 1998; accepted for publication Dec. 31, 1998.

*Visiting Researcher.
†Senior Researcher.
‡Senior Researcher. Associate Fellow AIAA.
§Professor, Mechanical Engineering Department, 242 CB.
¶Assistant Researcher.